Available online at www.sciencedirect.com
ScienceDirect
Radiation Measurements 43 (2008) 1017–1023
Radiation Measurements
www.elsevier.com/locate/radmeas

Invited paper

Properties of novel fluorescent nuclear track detectors for use in passive neutron dosimetry

G.J. Sykora[a,b], M. Salasky[c], M.S. Akselrod[a,*]

[a]*Landauer, Inc., Crystal Growth Division, 723 1/2 Eastgate St., Stillwater, OK 74074, USA*
[b]*Oklahoma State University, 145 PSII Stillwater, OK 74078, USA*
[c]*Landauer, Inc., 2 Science Rd, Glenwood, IL 60425, USA*

Abstract

A novel technique for neutron dosimetry has been developed using fluorescent nuclear track detectors (FNTDs) as a possible replacement for CR-39 plastic nuclear track detector (PNTD) technology. New aluminum oxide crystals containing aggregate oxygen vacancies and doped with carbon and magnesium (Al_2O_3:C,Mg) are imaged using laser scanning confocal fluorescence microscopy. Advancements in image processing allow for better detection of fluorescence tracks. Dose dependences were obtained for four types of neutron converters. A comparison between enriched ^{6}LiF (TLD-600) and LiF with natural abundance of ^{6}Li (TLD-100) was made. Dependence on angle of incidence for fast neutrons was investigated and compared with simulations based on neutron scattering theory. The reusability and re-readability of detectors were tested and confirmed to be satisfactory.

Keywords: Nuclear track detectors; Neutrons; Dose dependence; Aluminum oxide crystal; Laser-induced fluorescence; Confocal microscopy

1. Introduction

Plastic nuclear track detectors (PNTDs) and thermoluminescent detectors (TLDs) in albedo configuration are currently the most widely used dosimeters for personnel monitoring of fast and thermal neutrons. Landauer Inc. has recently developed novel fluorescent nuclear track detectors (FNTDs) as a technology suitable for replacing PNTD in neutron dosimetry and dosimetry of heavy charged particles (Akselrod et al., 2006a, b). The technology is a combination of a new luminescent aluminum oxide crystal, doped with carbon and magnesium (Al_2O_3:C,Mg) (Akselrod et al., 2003; Sanyal and Akselrod, 2005), with a technique based on laser scanning confocal fluorescence microscopy (Diaspro, 2002).

Al_2O_3:C,Mg crystals have green coloration (Fig. 1) due to a blue, 435 nm, absorption band formed by a new type of aggregate defect consisting of two oxygen vacancies and charge-compensated by two magnesium ions; these are F_2^{2+} (2Mg) color centers (Akselrod et al., 2003). F_2^{2+}(2Mg) centers efficiently capture the free electrons and undergo radiochromic transformation into a three-electron state forming F_2^{+}(2Mg) centers. If the F_2^{+}(2Mg) center is optically stimulated into one of its excited states, the electron will relax back to its ground state with a 75 ns lifetime, emitting a photon at 750 nm (Akselrod et al., 2003). It is important to emphasize that this process is not optically stimulated luminescence (OSL), which typically consists of two steps—photoionization of traps filled during irradiation and recombination of free charge carriers with luminescence centers. In FNTD technology we employ laser-induced fluorescence, which is intra-center luminescence produced as a result of an excitation and radiative relaxation process that occurs without photoionization of the color center. The result of irradiation is measured by detecting the intensity of radiation-induced fluorescence. The intensity is proportional to the number of radiochromically transformed F_2^{+}(2Mg) centers (Akselrod and Akselrod, 2006). The short 75 ns decay time of the F_2^{+}(2Mg) center makes it possible for fast laser scanning and imaging of the detector. Individual particle tracks appear as bright spots on a dark background.

* Corresponding author. Tel.: +1 405 377 5161; fax: +1 405 743 2966.
E-mail address: makselrod@landauerinc.com (M.S. Akselrod).

1350-4487/$ - see front matter © 2008 Elsevier Ltd. All rights reserved.
doi:10.1016/j.radmeas.2007.12.038

Fig. 1. Al_2O_3:C,Mg crystal and $4 \times 6 \times 0.5\,mm^3$ FNTD.

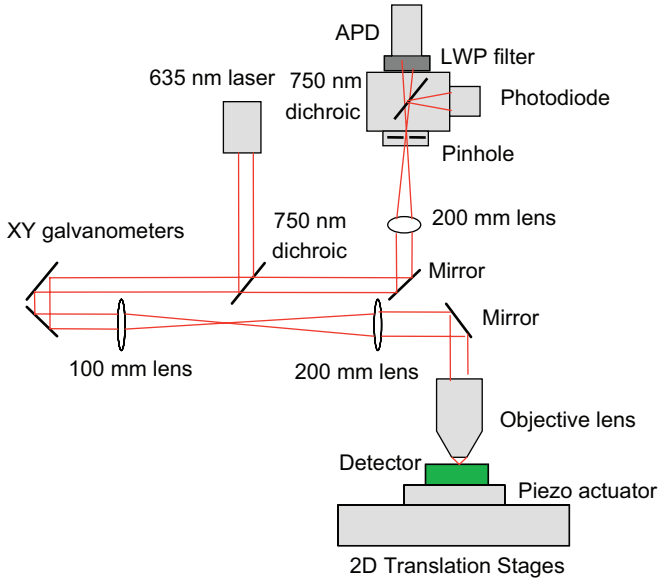

Fig. 2. Optical diagram of the FNTD confocal laser scanning imaging system.

2. Experimental

2.1. Materials and detector configuration

FNTD were cut from Al_2O_3:C,Mg single crystals in the form of $10 \times 6 \times 1$ and $6 \times 4 \times 0.5\,mm^3$ rectangular plates with the long side aligned along the optical *c*-axis of the crystal. One large side of the FNTD was polished. Because neutrons are not directly ionizing radiation and Al_2O_3 detectors are sensitive only to ionizing radiation, neutron converters mounted on top of them are necessary. In the case of fast neutrons, high density polyethylene (HDPE) is used because of its high concentration of hydrogen (Attix, 1986). Fast neutrons collide with bonded hydrogen atoms via elastic scattering and produce recoil protons which escape from the converter, penetrate the crystal and produce ionization. FNTD technology has been shown to detect charged particles with linear energy transfer (LET) in water as low as $0.5\,keV\,\mu m^{-1}$ (250 MeV protons) while maintaining the ability to measure charged particles with higher LET (Akselrod et al., 2006a and Sykora et al., 2007b). Therefore, detection of higher energy neutrons is possible.

In the case of thermal neutrons, there are a number of different materials with high thermal neutron capture cross-sections such as ^{6}LiF or ^{10}B. The corresponding nuclear reactions are as follows (the range in μm is for Al_2O_3):

$$^6\mathrm{Li} + {}^1\mathrm{n}(941\,\mathrm{barn}) \rightarrow {}^4\mathrm{He}(2.05\,\mathrm{MeV}, 4\,\mu\mathrm{m}) + {}^3\mathrm{H}(2.73\,\mathrm{MeV}, 24\,\mu\mathrm{m}), \quad (1)$$

$$^{10}\mathrm{B} + {}^1\mathrm{n}(3837\,\mathrm{barn}) \rightarrow {}^4\mathrm{He}(1.47\,\mathrm{MeV}, 3\,\mu\mathrm{m}) + {}^7\mathrm{Li}(0.83\,\mathrm{MeV}, 1.5\,\mu\mathrm{m}). \quad (2)$$

The alpha particle (^{4}He-ion) and tritium ion generated according to Eq. (1) have a maximum range in Al_2O_3 of 4 and 24 μm, respectively, and can be efficiently detected using FNTD technology because of the particles' higher energy and relatively longer range. The 1.5 MeV alpha particle in Eq. (2) has a range of only 3 μm and can still be detected, but with lower efficiency. The ^{7}Li ion produced in the ^{10}B reaction does not have enough range in Al_2O_3 to be detected. The advantage of ^{10}B is that its reaction cross-section is 4 times larger than that of ^{6}Li.

Multiple converter configurations were tested to determine the efficiency of fast and thermal neutron detection. The tested converters were 1 mm plates of HDPE, enriched ^{6}LiF (TLD-600 chips), LiF with natural abundance of ^{6}Li (TLD-100 chips) and ^{10}B loaded Teflon™. HDPE was used for its high concentration of hydrogen needed for production of recoil protons. TLD-600 chips were used for their large ^{6}Li concentration. LiF with natural abundance of ^{6}Li (TLD-100 chips) were tested as a converter to understand whether it could provide adequate track density and thermal neutron detection efficiency. Converters made of ^{10}B loaded Teflon® were investigated because of its high (n,α) reaction cross-section and its use in Landauer's CR-39 based neutron dosimeters.

2.2. Confocal imaging system

Fig. 2 depicts the optical diagram of the in-house built confocal scanning system designed to acquire fluorescence images from the detectors with diffraction limited resolution. In optical systems, the lateral resolution is defined as $0.61\lambda/NA$ and equal to 407 nm for the fiber-optically coupled diode laser with a wavelength $\lambda = 635$ nm and high numerical aperture (NA) 40X, 0.95NA objective lens. Two-axis galvanometer mirrors are used for a high scanning rate in the XY plane. Axial (Z) scanning and focal point depth positioning in the crystal is provided by a piezo-actuator stage. The fluorescence excited by the laser light is collected by the same objective lens, transmitted back through the dichroic mirror, imaged on a confocal

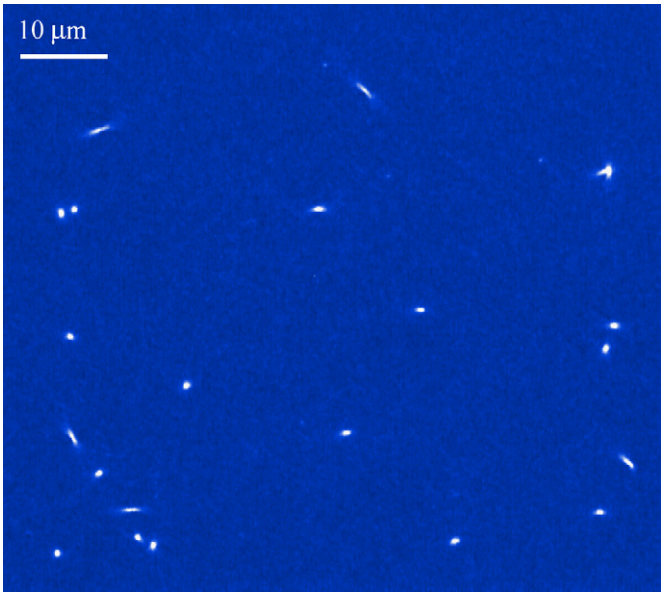

Fig. 3. $85 \times 85\,\mu m^2$ fluorescence image of recoil proton tracks acquired from an FNTD after irradiation with 60 mSv of fast neutrons.

pinhole and detected by a silicon avalanche photodiode (APD) installed behind the pinhole. An additional optical filter in front of the APD rejects residual laser light. The confocal pinhole is a spatial filter, blocking all fluorescence originating outside of the focal spot of the objective lens and providing diffraction limited spatial discrimination. Images are formed as an array of voltages obtained by the data acquisition board from the photodetector. Fig. 3 is a typical image produced after 60 mSv of Am-Be fast neutron irradiation.

After images are obtained, they are processed using automatic image processing software developed in a LabView™ programming environment. Tracks are identified and counted by the software giving the overall particle fluence. The sensitivity of the detectors is defined as number of tracks per 1 mSv and per 1 mm^2 of the detector area.

2.3. Irradiations

Neutron irradiations were performed at the Landauer irradiation facility in Glenwood, IL, using unmoderated and moderated Am-Be sources. Irradiations with fast neutrons were performed using a 185 MBq Am-Be source in two geometries: "free-in-air" at 20 cm from the source and on a $30 \times 30 \times 15\,cm^3$ PMMA phantom at 50 cm distance. Thermal and epithermal neutrons were produced by a 37 MBq Am-Be source moderated by 180 mm of paraffin. The dose rate of moderated neutrons was determined using a gold foil activation technique. The contribution of fast neutrons in this source configuration is still significant. The results for moderated AmBe source presented in this study show that the contribution to dose equivalent of fast neutrons is more than 5 times the contribution due to thermal and epithermal neutrons. The delivered dose range was between 0.3 and 300 mSv for fast neutrons and 0.3 and 10 mSv for moderated neutrons.

Because TLD-100 has a natural abundance of ^{6}Li, multiple detectors with a total of seven TLD-100 converters chosen from random lots were exposed to 0.3, 1 and 3 mSv of moderated neutron doses to investigate the stability of ^{6}Li content and consistency of neutron conversion. Fourteen other detectors covered by HDPE were irradiated with the same unmoderated 185 MBq Am-Be source under different angles with respect to the direction of fast neutron incidence. The detectors were placed on wedged pieces of plastic that were machined to have the angle between the detector and the incident neutron beam vary from 0° (the detector surface is perpendicular to the incident beam) to 90° (the detector's front surface is parallel to the incident neutron beam) in 15° increments. Two detectors were irradiated at each of the seven angles. All 14 detectors were irradiated at the same time and received a dose of 6 mSv.

FNTD produced from different crystals were routinely imaged for quality assurance and sensitivity check after irradiation in vaccum with 5.1 MeV alpha particles from a 1 μCi ^{241}Am source located 12 cm from the detector surface. Alpha particles incident on the crystal from this distance in vacuum penetrate almost perpendicular to the detector surface. The alpha particles are not absorbed by air and create round tracks of identical amplitudes.

After irradiation, the detector is first scanned perpendicular to the detector surface using a piezoelectric actuator to detect the surface position with an accuracy of 100 nm. After finding the axial surface position, the detector is scanned in a plane parallel to its surface—usually at a depth of 2 μm below the surface. The imaged area usually has dimensions of up to $150 \times 150\,\mu m^2$. Multiple images spaced 10 μm apart from each other were obtained from each FNTDs behind each of the converters. The number of acquired images depended on the measured dose and was adaptively varied between 5 and 40 for each of the converter areas. All images were automatically processed to obtain a track count and to calculate track density and dose. Tracks were periodically counted manually for quality control.

3. Results and discussion

3.1. Dose dependence

The dose determined by FNTD is proportional to the measured track density:

$$D = (N' - B)/S, \tag{3}$$

where $N' = f(N)$ is the measured track density corrected for linearity deficiency, B is the background, both in tracks mm^{-2} and S is the detector sensitivity in tracks $mm^{-2}\,mSv^{-1}$.

The track density for all irradiated detectors was obtained from 5 to 40 images per detector and was adjusted depending on the number of tracks per image to ensure good statistical precision. All obtained dose dependences (Fig. 4) show good linearity within at least three orders of investigated dose range. There is no difference in sensitivity of FNTD behind HDPE converter between irradiations performed in-air and on-phantom (Fig. 4a), which indicates that albedo neutrons do not significantly affect the sensitivity of the detectors to fast neutrons. Large error in

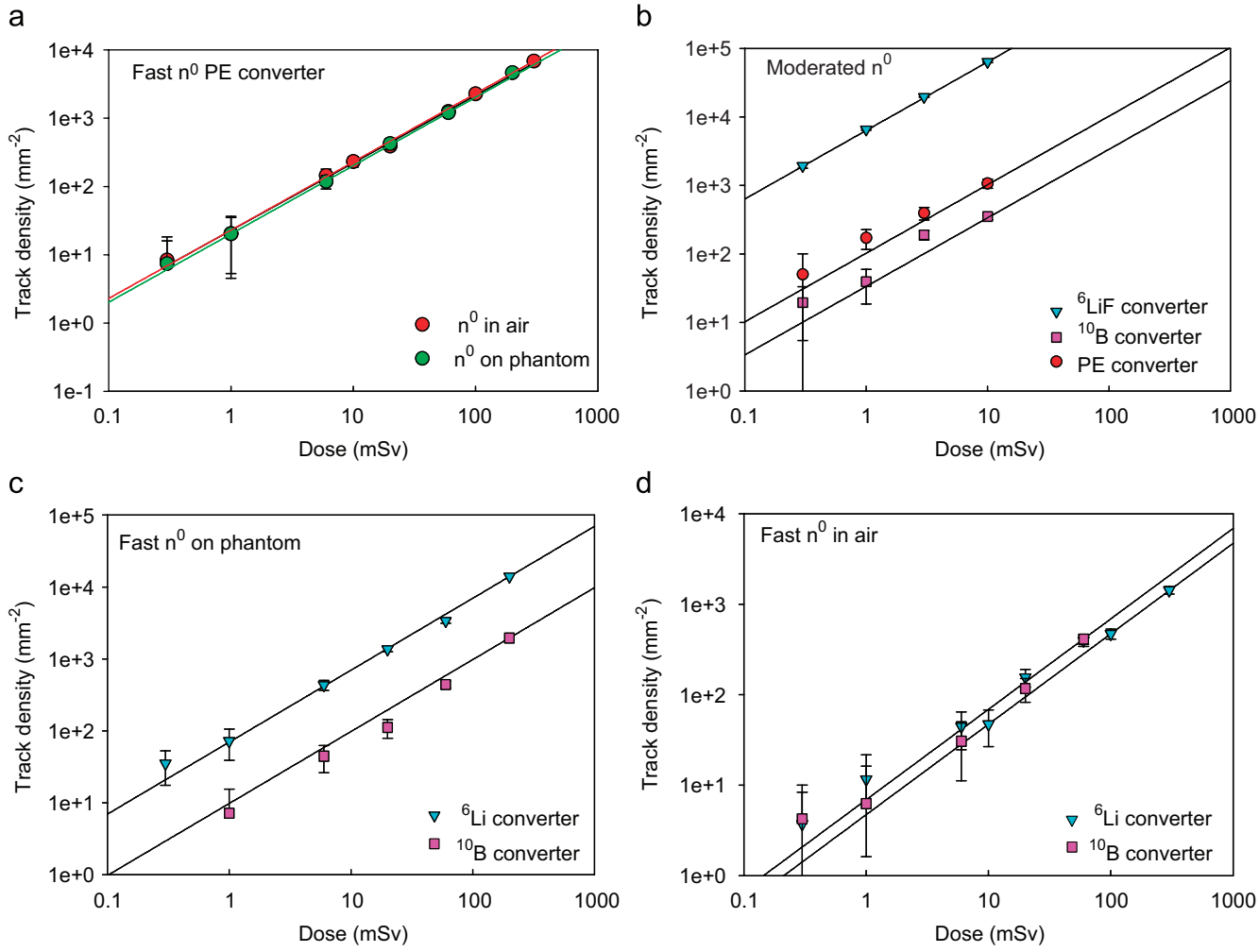

Fig. 4. Dose dependences of track densities for FNTDs covered with three different converters and irradiated with Am-Be sources.

low doses is a result of low track density. The error can be reduced by imaging more frames for better statistics.

The sensitivity S to fast neutrons obtained from the FNTD-HDPE detector configuration is 21.5 tracks mm^{-2} mSv^{-1} and is consistent with preliminary results (Akselrod et al., 2006b and Sykora et al., 2007a). In comparison, the sensitivity of CR-39 to fast neutrons is 12.1 tracks mm^{-2} mSv^{-1}. The difference in sensitivity is most likely due to the FNTD's better sensitivity to lower LET charged particles (higher energy protons) and its ability to detect tracks incident at grazing angles. The sensitivity of FNTD to thermal neutrons with ^{6}LiF (TLD-600) as a converter (Fig. 4b) is 6500 tracks mm^{-2} mSv^{-1}, which is also consistent with the sensitivity reported previously (Akselrod et al., 2006b and Sykora et al., 2007a). The track density per 1 mSv of dose for the thermal component of FNTD obtained using TLD-600 is 300 times higher than the HDPE component, making the thermal component almost insensitive to fast neutrons. As a result, it was concluded that the HDPE component of the detector is effectively sensitive only to fast neutrons, whereas the TLD-600 converter provides response effectively exclusive to the moderated neutron component of the radiation field. For neutrons moderated by paraffin with a large thermal component, the ^{6}LiF converter provides 100 times higher response than the ^{10}B-loaded Teflon® converter (5% of ^{10}B by weight) commercially used in combination with Landauer CR-39 detectors (Fig. 4b). ^{10}B as a converter of thermal neutrons has higher capture cross-section than ^{6}Li (3840 and 940 barn, respectively), but the latter one produces two charged particles with higher Q value and larger particle ranges. In contrast, the results from "free-in-air" fast neutron irradiations show their sensitivity to be almost equal (Fig. 4d). The albedo configuration during on-phantom irradiations shows the intermediate situation (Fig. 4c).

Results presented in Figs. 4c and d from thermal components of the FNTD indicate significant amounts of scattered and moderated neutrons present in the fast neutron field with and without phantom behind the FNTD. In turn, the track density obtained behind the HDPE converters after irradiation with the moderated Am-Be source (see Fig. 4b) indicates significant amount of fast neutrons in the moderated field. The estimated contribution to dose equivalent of fast neutrons is more than 5 times the contribution due to thermal and epithermal neutrons.

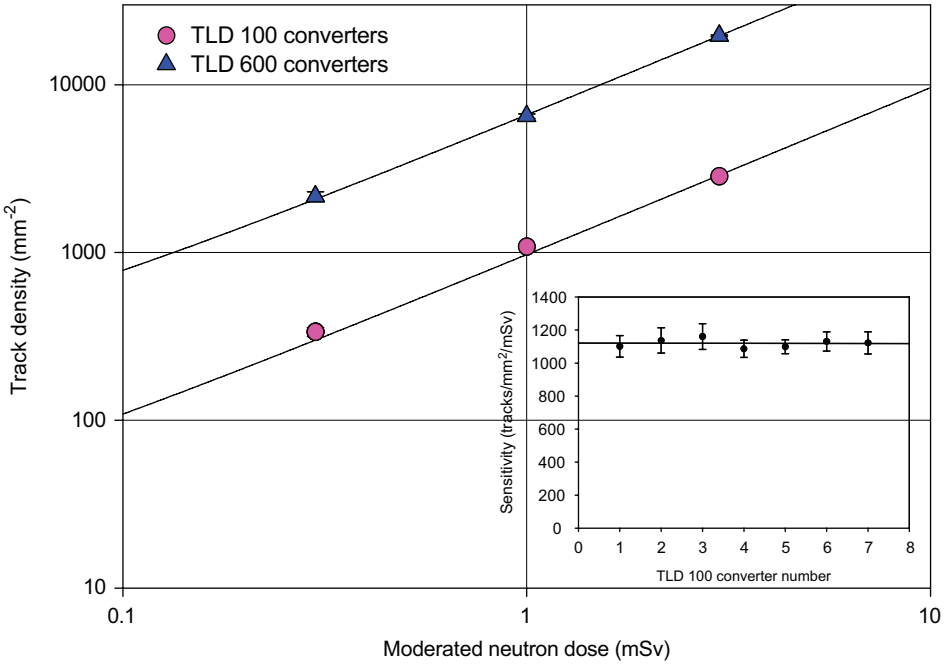

Fig. 5. Dose dependences for FNTD with LiF TLD-100 and TLD-600 chips used as moderated neutron converters. The insert demonstrates variability in moderated neutron sensitivity for seven FNTDs with seven different TLD-100 chips as neutron converters.

The sensitivity of FNTD with a TLD-100 converter to moderated neutrons was 1100 tracks mm^{-2} mSv^{-1}, a factor of 6 less than for TLD-600 (Fig. 5). This sensitivity is still high enough to detect thermal doses reliably and has an advantage of a higher saturation dose by the same factor of 6. In FNTD technology, the maximum measurable track density and corresponding dose are limited by the overlap of tracks. In comparison with CR-39, the track area in FNTD is approximately 100 times lower, which translates to a higher detectable track density.

One of the concerns with using TLD-100 as a neutron converter is consistency of ^{6}Li abundance in LiF chips produced from different lots of material. Inconsistency of ^{6}Li content could lead to a change in dosimeter sensitivity in terms of tracks mm^{-2} mSv^{-1}. It is for this reason that multiple FNTDs combined with TLD-100 chips from a random selection of lots were tested with a neutron dose of 0.3 mSv. The insert in Fig. 5 demonstrates the variability in sensitivity among seven different FNTD and TLD-100 chips. The deviation in sensitivity is 2.3% from the mean which is not statistically significant.

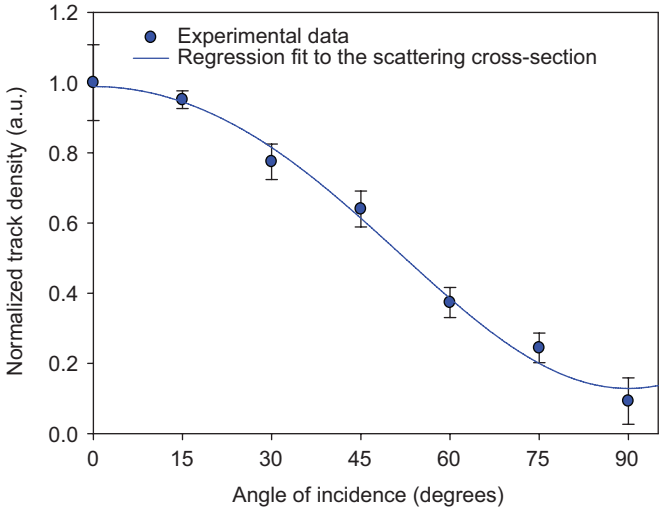

Fig. 6. Angular dependence of FNTD response obtained after irradiations with 6.0 mSv of fast neutrons from an unmoderated Am-Be source. The data are normalized to zero angle of incidence. The solid line represents the fit of the experimental data to Eq. (7).

3.2. Angular dependence

FNTD with HDPE converters were irradiated with a fast neutron dose of 6 mSv at angles of incidence from 0° to 90° in 15° increments. The detectors were mounted on two plastic substrates with multiple angles on each substrate. It is evident from the dose dependence of detectors combined with HDPE and irradiated on phantom (Fig. 4a) that there is no significant contribution to the number of tracks from albedo neutrons whether there is a plastic phantom behind the detector or not. Fig. 6 is the normalized track count dependence on angle of incidence for FNTD irradiated with fast neutrons.

The track count for all angles of irradiation was normalized to the track count obtained for the direction of incidence normal to the detector surface. The angular dependence obtained was fitted to Legendre polynomials in accordance with recent experiments and Monte Carlo calculations on n–p scattering cross-sections for neutron energies below 15 MeV

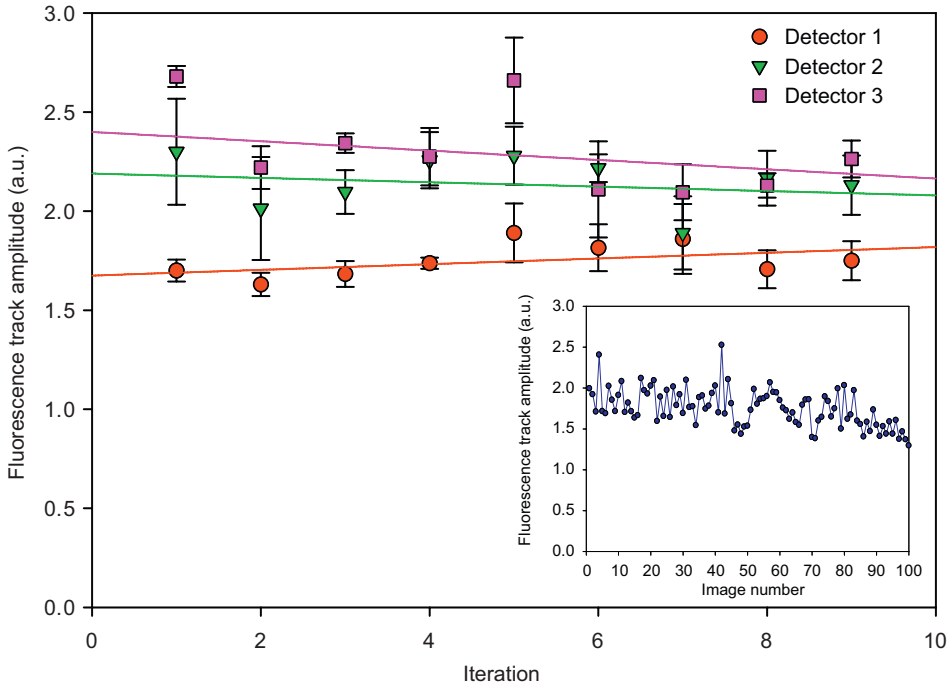

Fig. 7. Reusability test showing no significant change in detector sensitivity and fluorescence track amplitude. The insert illustrates the results of 100 consecutive readouts of the same area of the detector irradiated with alpha particles.

(Boukharaouba et al., 2001). According to the study, Legendre polynomials for the angular dependence of the n–p scattering cross-section, σ_s, in the center-of-mass frame is given by

$$\sigma_s(\Theta_{cm}) = a_0 + a_1 P_1(\cos\Theta_{cm}) + a_2 P_2(\cos\Theta_{cm}), \quad (4)$$

where Θ_{cm} is the angle of the scattered proton with respect to the angle of incidence of the neutron and a_0, a_1 and a_2 are parameters and $P_i(\cos\Theta_{cm})$ are Legendre polynomials of order i and are given by

$$P_1(\cos\Theta_{cm}) = \cos\Theta_{cm},$$
$$P_2(\cos\Theta_{cm}) = \tfrac{1}{2}(3\cos^2\Theta_{cm} - 1). \quad (5)$$

From simple scattering theory we can change the reference frame to the lab frame by

$$\cos\theta = \sqrt{\frac{1-\cos\Theta_{cm}}{2}}, \quad (6)$$

where θ is the scattering angle of the recoil proton in the lab frame. Plugging (5) and (6) into (4) and absorbing the constants, we are left with the scattering cross-section in the lab frame, $\sigma_s(\theta)$ given by

$$\sigma_s(\theta) = b_0 + b_1\cos^2\theta + b_2\cos^4\theta, \quad (7)$$

where b_0, b_1 and b_2 are fitting parameters. Regression analysis of experimental results (Fig. 6) with the regression coefficient $R^2 = 0.992$ suggests that the angular dependence of FNTD is well described by the theoretical dependence of the n–p scattering cross-section.

3.3. Reusability and re-readability

The reusability of three detectors cut from three different crystals was tested. The detectors were irradiated in vacuum with 5.1 MeV alpha particles from a ^{241}Am source. The detectors were imaged, tracks were counted and the fluorescence amplitudes of the tracks were measured. After the measurements, the detectors were erased by thermal annealing to 680 °C and slowly cooled to return the detector to its original state (before the next irradiation). The detectors were read after annealing to make sure that the tracks were completely erased. This process was then repeated 9 times. Fig. 7 shows the average fluorescence amplitude of the alpha particle tracks obtained after every irradiation and it does not indicate any statistically significant degradation in fluorescence track amplitude.

To demonstrate re-readability, one detector irradiated with alpha particles was scanned 100 times in the same area. Each image was processed to measure the fluorescence amplitude of the alpha particle tracks. As seen in the insert in Fig. 7, there is no significant degradation of track amplitude until the 80th readout. This demonstrates that the readout process is almost completely non-destructive. There is slight erasure of both background fluorescence and the track fluorescence amplitude at very long laser light exposure time. This might be caused by a finite probability of three-photon absorption process.

4. Conclusions

Fluorescent nuclear track detectors based on Al_2O_3:C,Mg single crystals are suggested as a new technology for neutron

dosimetry. The readout process of FNTD is completely optical and non-destructive, allowing for multiple readouts of the same detector. It eliminates chemical etching needed for processing of CR-39. FNTDs also allow for fast automatic scanning, image processing and track counting.

Dose dependences were obtained for several FNTD-converter combinations. The dose response was linear throughout the entire range of investigated doses for both fast and thermal neutrons. It was also demonstrated that FNTDs have high sensitivity and good fast to thermal neutron discrimination. The relatively large errors at the low doses can be reduced by imaging a larger amount of frames for better statistics. Smaller track size provides a saturation dose that is more than 100 times higher than for CR-39 PNTD and the neutron detection efficiency of FNTD is 2 times higher.

A comparison between two types of moderated neutron converters was performed: TLD-100 chips with a natural abundance of ^{6}Li and TLD-600 chips with 95% enriched ^{6}Li content. It was shown that TLD-100 chips can be used as a reliable, cost-effective, thermal neutron converter allowing higher thermal neutron doses to be measured.

Angular dependence was shown to follow the theory based on the n–p scattering model. The reusability of FNTD after thermal annealing was demonstrated for nine consecutive irradiations. Re-readability of the same detector was demonstrated for 100 consecutive reads.

Acknowledgments

We would like to thank our colleagues T.H. Underwood, K.J. Dillin and J. Allen for their contributions to the development of crystal growth technology and sample preparation.

References

Akselrod, G.M., Akselrod, M.S., Benton, E.R., Yasuda, N., 2006a. A novel Al_2O_3 fluorescent nuclear track detector for heavy charged particles and neutrons. Nucl. Instrum. Methods B 247, 296–306.

Akselrod, M.S., Akselrod, A.E., 2006. New Al_2O_3:C,Mg crystals for radiophotoluminescent dosimetry and optical imaging of tracks produced by heavy charge particles. Radiat. Prot. Dosim. 119 (1–4), 218–221.

Akselrod, M.S., Akselrod, A.E., Orlov, S.S., Sanyal, S., Underwood, T.H., 2003. Fluorescent aluminum oxide crystals for volumetric optical data storage and imaging applications. J. Fluoresc. 13 (6), 503–511.

Akselrod, M.S., Yoder, R.C., Akselrod, G.M., 2006b. Confocal fluorescent imaging of tracks from heavy charged particles utilizing new Al_2O_3:C,Mg crystals. Radiat. Prot. Dosim. 119 (1–4), 357–362.

Attix, F.H., 1986. Introduction to Radiological Physics and Radiation Dosimetry. Wiley, New York, NY.

Boukharaouba, N., Bateman, F.B., Brient, C.E., Carlson, A.D., Grimes, S.M., Haight, R.C., Massey, T.N., Wasson, O.A., 2001. Measurement of the n–p elastic scattering angular distribution at $E_n = 10$ MeV. Phys. Rev. C 65, 014004.

Diaspro, A. (Ed.), 2002. Confocal and Two-Photon Microscopy: Foundations, Applications, and Advances. Wiley, New York.

Sanyal, S., Akselrod, M.S., 2005. Anisotropy of optical absorption and fluorescence in Al_2O_3:C,Mg crystals. J. Appl. Phys. 98, 033518.

Sykora, G.J., Akselrod, M., Salasky, M., Marino, S.A., 2007a. Novel Al_2O_3:C,Mg fluorescence nuclear track detectors for passive neutron dosimetry. Radiat. Prot. Dosim., published on-line, May 23, 2007, doi:10.1093/rpd/ncm058.

Sykora, G.J., Akselrod, M.S., Benton, E.R., Yasuda, N., 2007b. Spectroscopic properties of novel fluorescent nuclear track detectors for high and low LET charged particles. Radiat. Meas. (this issue), doi:10.1016/j.radmeas.2007.11.009.